NANO LETTERS

pubs.acs.org/NanoLett Letter

Multifunctional Superelastic Graphene-Based Thermoelectric Sponges for Wearable and Thermal Management Devices

Ding Zhang, Yin Mao, Peijia Bai, Qi Li, Wen He, Heng Cui, Fei Ye, Chenxi Li, Rujun Ma,* and Yongsheng Chen*

Cite This: *Nano Lett.* 2022, 22, 3417−3424 Read Online

ABSTRACT: Power generation through harvesting human thermal energy provides an ideal strategy for self-powered wearable design. However, existing thermoelectric fibers, films, and blocks have small power generation capacity and poor flexibility, which hinders the development of self-powered wearable electronics. Here, we report a multifunctional superelastic graphene-based thermoelectric (TE) sponge for wearable electronics and thermal management. The sponge has a high Seebeck coefficient of 49.2 μV/K and a large compressive strain of 98%. After 10 000 cyclic compressions at 30% strain, the sponge shows excellent mechanical and TE stability. A wearable sponge array TE device was designed to drive medical equipment for monitoring physiological signals by harvesting human thermal energy. Furthermore, a 4 × 4 array TE device placed on the surface of a normal working Central Processing Unit (CPU) can generate a stable voltage and reduce the CPU temperature by 8 K, providing a feasible strategy for simultaneous power generation and thermal management.

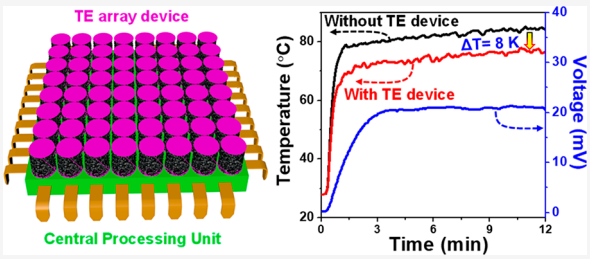

KEYWORDS: *Seebeck effect, Graphene sponge, Wearable, Thermal energy harvesting, Thermal management*

Flexible thermoelectric (TE) materials have shown great potential in providing continuous power to wearable electronics due to the ability to convert thermal energy into electricity based on the Seebeck effect.[1−6] But the limitations of traditional batteries and capacitors as power sources, partially because of the inconvenience caused by their rigidness and frequent maintenance and charging requirements,[7−9] renders more and more researchers to design and study flexible TE materials and devices. However, due to the theoretical limit of TE conversion efficiency, the reported flexible TE materials have difficulty meeting the actual demand of low-power electronic devices.[10−13] Therefore, the development of self-powered wearable electronics still faces huge challenges. To improve the TE output, it is common to design TE devices with array structures by making full use of thermal energy based on traditional inorganic TE materials.[14−18] A typical example is the integration of inorganic P-/N-Bi_2Te_3 materials into flexible polymer substrates as TE legs with high integration.[19−21] As intrinsically flexible TE materials, conductive polymer TE fibers have exhibited great potential in the manufacture of electronics fabric for wearable devices.[22−24] However, the above-mentioned design scheme usually relies on microprocessing technology and a complex material preparation technique, resulting in a complicated preparation process and high cost. In addition, the traditional and commercial inorganic TE materials tend to be rigid and brittle, restricting their feasibility in small-scale and built-in applications.

TE systems based on carbon nanotubes (CNTs) and graphene have been proposed as an efficient alternative to realize self-powered devices due to their extraordinary electronic transport properties.[25−35] While effective for many applications, carbon nanomaterials have difficulty meeting the power demands of modern technologies, such as wearable and flexible electronics. Through structure design, several CNT-based TE fibers and graphene-based TE films were fabricated as wearable electronic devices for thermal energy harvesting. However, the small Seebeck coefficient limits their applications[36,37] due to the remarkable thermal conductivity of their special low dimensional structure leading to the relatively low-temperature difference and TE output.[26,38] In the case of graphene, although there are many efforts to improve the TE properties of graphene by designing different structures or chemical treatments, the realization of practical self-powered devices remains a major challenge.[26,39−44] Inspired by the aerogels with a three-dimensional (3D) porous structure,[45] the

Received: February 19, 2022
Revised: April 6, 2022
Published: April 11, 2022

https://doi.org/10.1021/acs.nanolett.2c00696
Nano Lett. 2022, 22, 3417−3424

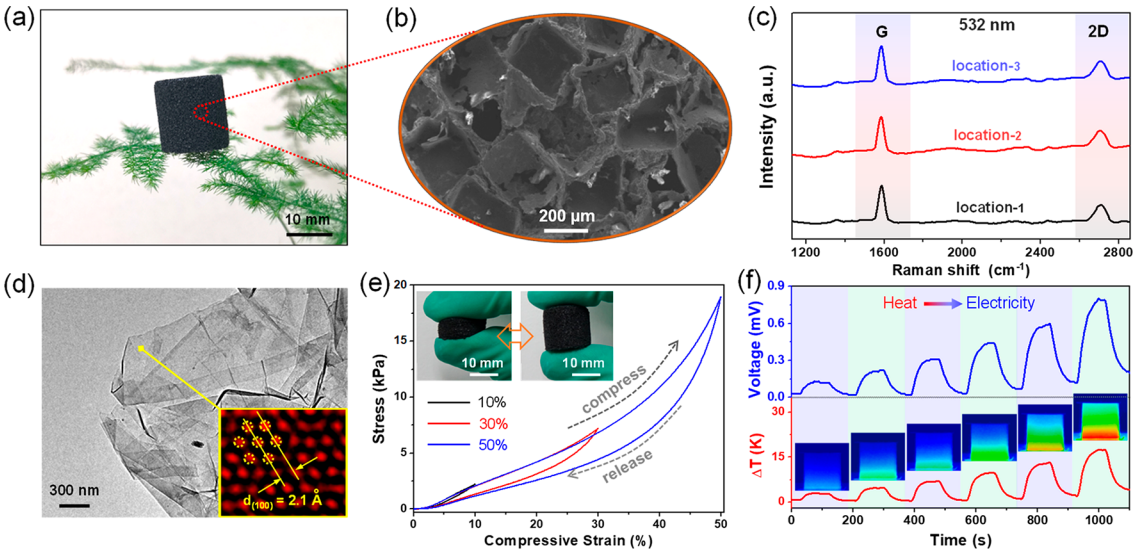

Figure 1. Characterization and properties of the TE sponges. (a) Optical image of a leaf supporting a TE sponge. (b) SEM image of the sponge. (c) Raman spectra of the graphene sheets under a 532 nm excitation wavelength. (d) TEM image of the graphene sheets and corresponding high-resolution TEM image. (e) Stress−strain curves at different compressive strains from 10% to 50%, the inset showing the compressibility and recoverability. (f) The output voltage of the TE sponge was measured under various ΔT, the inset showing the infrared images of the TE sponge under six stable ΔT values.

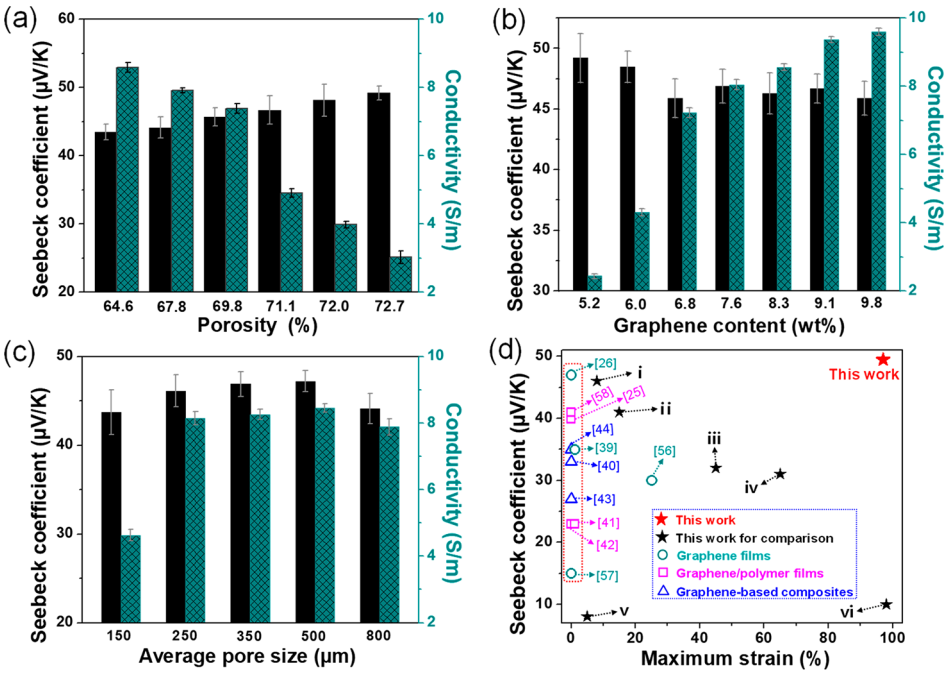

Figure 2. Optimization of TE properties. (a) Seebeck coefficient and electrical conductivity of the TE sponges with different porosities. (b, c) Seebeck coefficient and electrical conductivity with different graphene contents (b) and different pore sizes (c). (d) Comparison of the maximum Seebeck coefficient and strain of the seven graphene-based TE sponges in this work and previously reported raw graphene-based TE films. Note: The marks "i−vi" are expressed as graphene/PVA, graphene/PVDF, graphene/Ecoflex, graphene/Rcoflex, graphene/PU, and RGO sponges, respectively.

heat transfer performance can be controlled by the design of the porous structure.[46−49] Therefore, high TE and mechanical properties can be achieved through 3D structure design. Additionally, thermal energy is gradually consumed during the TE conversion process and the carbon-based TE materials have relatively high emissivity, so it is expected to realize high-efficiency power generation and thermal management simultaneously.

In this work, we report a multifunctional superelastic graphene-based TE sponge with a high Seebeck coefficient of 49.2 μV/K and a large compressive strain of 98%. The sponges can realize self-powered temperature and strain sensing with high sensitivity. As a wearable device, the TE sponge array integrated into the insole can efficiently collect human thermal energy due to the temperature difference between the foot and the ground. The produced electricity can drive low-power medical equipment for monitoring physiological signals.

https://doi.org/10.1021/acs.nanolett.2c00696
Nano Lett. 2022, 22, 3417−3424

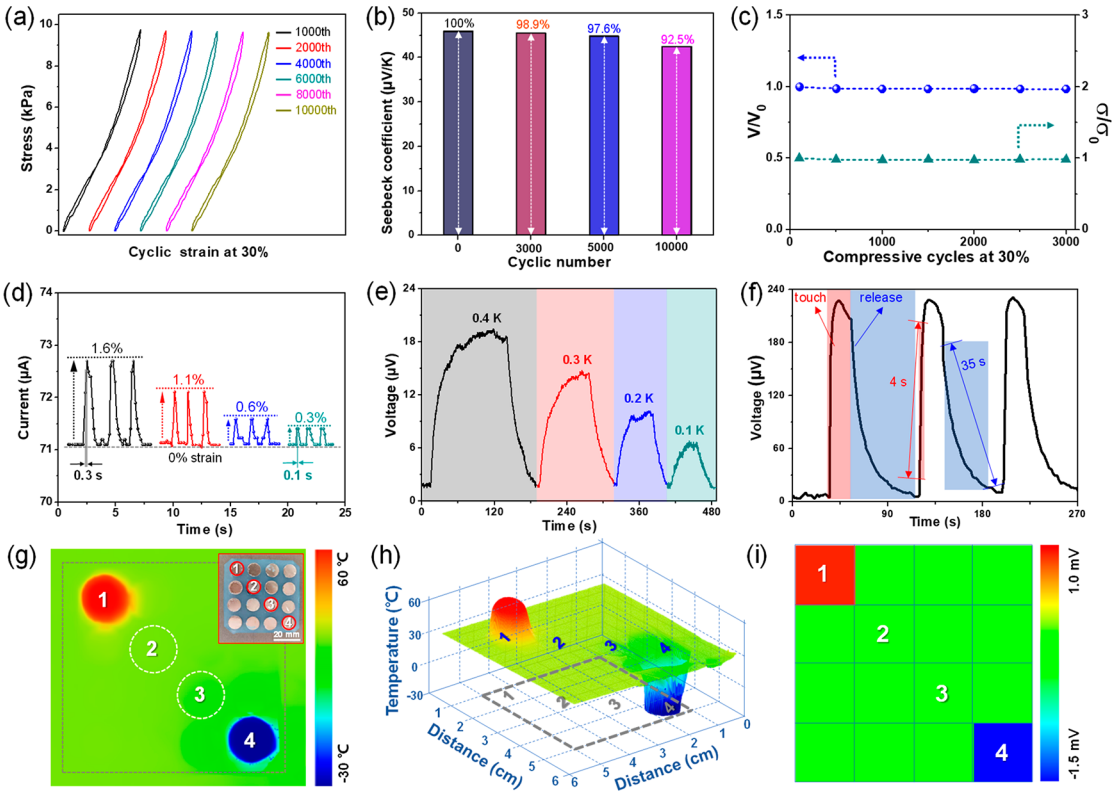

Figure 3. Stability measurement and strain/temperature sensing performance. (a) Stress−strain curves of the TE sponge at the cyclic strains from 0% to 30% for 10 000 cycles. (b) Comparison of the Seebeck coefficient of the sponge under different cyclic numbers at the compressive strains of 30%. (c) Relative changes of the output voltage and electrical conductivity during the 3000 cyclic compressive strain at 30%. (d) Small compressive strain-induced current variations caused under the ΔT of 16 K. (e) Voltage response of the TE sponge for detecting small ΔT in a sequence of 0.4, 0.3, 0.2, and 0.1 K. (f) Voltage response of the TE sponge to finger touching. (g−i) Infrared images of 2D (g) and 3D (h) and the corresponding voltage mapping image (i) of the multichannel 4 × 4 array TE sensing system, where a hot iron disk and a cold iron disk are put on Sensor-1 and Sensor-4, respectively.

Moreover, a 4 × 4 array TE device on the surface of a normal working CPU can produce a stable TE voltage and reduce the CPU temperature. The multifunctional compact TE device demonstrated here not only leapfrogs the property of existing flexible TE technologies but also brings flexible TE devices closer to reality for a variety of practical applications that require self-powered and thermal management devices.

Figure S1 shows the preparation of the TE sponge, and the sodium chloride (NaCl) cubes act as pore-forming additives.[50,51] After immersing the prepared graphene/PDMS/NaCl composite block in hot water, the NaCl cubes are dissolved in the hot water to form a porous graphene/PDMS sponge. Figure 1a shows the photograph of a typical TE sponge with a porosity of 69.8% and graphene content of 6.8 wt % supported by an asparagus fern leaf and corresponding microstructure, indicating the extreme light weight of the sponge with an average pore size of ∼250 μm (Figure 1b). In addition, an aluminum (Al) block with a mass of 180 g can be supported by a small cylindrical TE sponge (8 mm in radius and 16 mm in height) as shown in Figure S2a, which exhibits the relatively high strength of the TE sponge. The scanning electron microscopy (SEM) analysis indicates that the raw graphene sheets have a large lateral size with a wrinkled structure (Figure S2b). The Raman spectra of the graphene sheets were characterized under an excitation wavelength of 532 nm at room temperature (Figure 1c). The intensity ratios $I_{G/2D}$ of the G band to the 2D band at three locations are all between 2.0 and 2.2, which indicates that the raw graphene sheets are 3−4 layers in thickness.[52] Figure 1d exhibits the TEM image of the raw graphene sheets, further confirming the few-layer structure. Moreover, through the high-resolution TEM image in the inset of Figure 1d, the interplanar spacing of the graphene sheets is estimated to be 2.1 Å, which corresponds to the (100) plane of hexagonal graphite (JCPDS No. 75-1621).[53,54] Compression tests indicate the TE sponge shows excellent recoverability, cyclic stability, and linear relationship between resistance and compressive strain (Figure 1e, S3a,b, Note S1). To investigate the TE performance of the graphene-based sponge, a commercial heating platform was utilized to establish a stable temperature gradient in the height direction. The top and bottom electrodes of the cylindrical TE sponge were copper plates. All temperature distribution and the temperature difference (ΔT) curves of the TE sponge were recorded by an infrared (IR) camera. By controlling the heating platform temperature, six stable temperature gradients can be obtained between two copper electrodes in the inset of Figure 1f. The output voltage variation and linear fitting curve are shown in Figure 1f and Figure S3c, which indicates the output voltage is proportional to the ΔT between two electrodes. According to the calculation formula of the Seebeck coefficient, $S = -dV/dT$, the slope of the fitting curve represents the Seebeck coefficient of the TE sponge.

Considering that the porous structure may affect the thermal conductivity,[38,55] we studied the mechanical and electrical properties of the TE sponges with different porosities (Figures

https://doi.org/10.1021/acs.nanolett.2c00696
Nano Lett. 2022, 22, 3417−3424

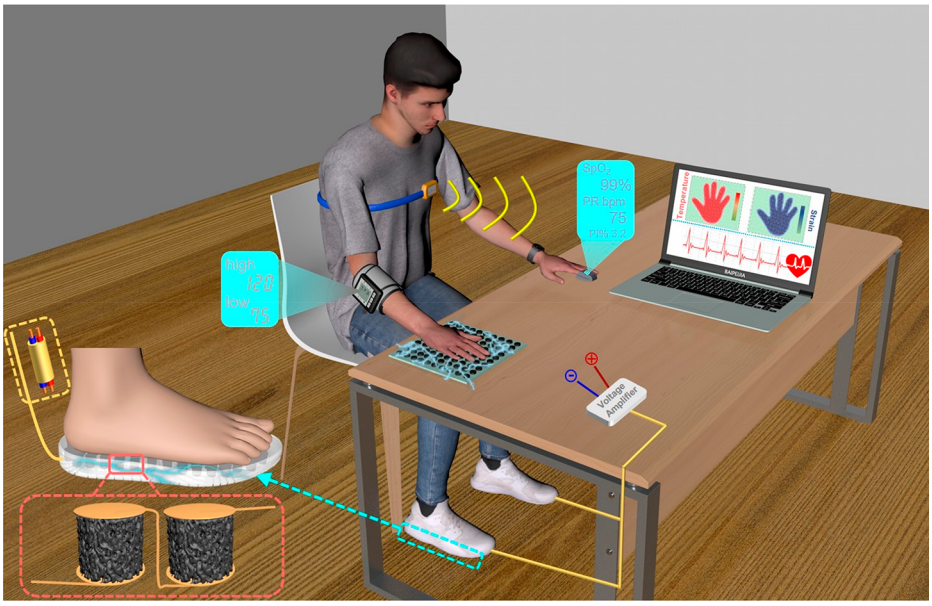

Figure 4. Potential application scenarios of TE sponges as wearable electronics in daily life. The fabricated TE sponges are expected to be used in daily life through harvesting human thermal energy, showing huge application potential in self-powered temperature/strain sensing and driving low-power medical electronics for physiological signal monitoring.

S4 and S5, Note S2). As observed in Figure 2a, the average Seebeck coefficient of the TE sponge gradually increases from 43.5 to 49.2 μV/K with an increase of porosity from 64.6% to 72.7%. Meanwhile, both the electrical and the thermal conductivities decrease with the increase of porosity since more pores can reduce the conductive path in the TE sponge (Figure 2a and Figure S6). The decrease of thermal conductivity shows a positive effect on improving the Seebeck coefficient, while the power factor (PF) is gradually decreased. To further optimize the TE performance of the sponges, we further systematically studied the effect of graphene content and pore sizes on the TE performance of the TE sponges (Figure 2b,c). It is found that the optimal TE sponges have a porosity of 69.8%, graphene content of 7.6%, and average pore size of ~500 μm, corresponding to the optimized Seebeck coefficient of 47.2 μV/K and electrical conductivity of 8.45 S/m (Figure S7a,b, Note S3). Figure 2d compares the Seebeck coefficient and the maximum stretchable/compressive strain of the 3D graphene-based TE sponges with other graphene TE materials, including the raw graphene films,[26,39,56,57] graphene−polymer films,[25,41,42,58] and graphene-based composites.[40,43,44] Herein, most of the works reported in the literature have not studied the tensile or compressive properties of graphene-based TE materials, as marked in the red dotted box of Figure 2d. To facilitate the comparison of mechanical properties, we assume that the tensile or compressive strain of these materials is very small and even close to zero. It is observed that our fabricated graphene/PDMS TE sponge reaches a maximum average Seebeck coefficient of ~49.2 μV/K and an extraordinarily compressive strain as high as 98%, which is larger than that of any reported graphene-based TE materials. For comparison, we also investigated the TE and compressive properties of reduced graphene oxide (RGO) sponge and five other graphene/polymer sponges in this work. It is observed that the graphene/PVA sponge shows relatively good TE performance and poor compressive property, while the RGO sponge is the opposite. Compared with the above six TE sponges, the best TE and mechanical properties of the graphene/PDMS sponge are attributed to the beneficial interfacial interaction between graphene sheets and PDMS precursor molecular chains.

Through the above performance optimization, we selected the TE sponge with a porosity of 69.8%, a graphene content of 7.6%, and an average pore size of ~500 μm for the following studies. According to the cyclic stress−strain curves shown in Figure 3a and the time-dependent stress variation (Figure S8), the TE sponge exhibits excellent mechanical and TE stability within 10 000 cycles at the compressive strain of 30% without obvious performance degradation. The retention rates of the Seebeck coefficient are up to 98.9%, 97.6%, and 92.5%, corresponding to the cyclic numbers of 3000, 5000, and 10 000, respectively (Figure 3b). In addition, both the output voltage and electrical conductivity (σ) of the TE sponge remain almost constant during the 3000 cycles of strain from 0 to 30% at a ΔT of 16 K (Figure 3c). The electrical output and Seebeck coefficient of the TE sponge were systematically measured when the compressive strain increased from 0 to 30% under a constant ΔT of 16 K (Figure S9, Note S4). By controlling the ΔT fixed at 16 K, we investigated the current change caused by several small compressive strains. The cyclic small strains can cause cyclic current changes (Figure 3d), and the TE sponge can monitor an ultrasmall strain up to 0.3% with a response time less than 0.1 s, indicating the excellent sensing performance with high strain resolution and fast response.

Except for excellent strain sensing ability, the fabricated TE sponge can realize self-powered temperature sensing due to the Seebeck effect. By controlling the working voltage of a heating platform, small ΔT values of 0.4, 0.3, 0.2, and 0.1 K across the height direction of the TE sponge were achieved. Figure 3e gives the corresponding time-dependent voltage curve under a decreased ΔT from 0.4 to 0.1 K. The monitored minimum ΔT is only 0.1 K, showing the excellent potential application in sensing an extremely small temperature difference. When a fingertip touches the TE sponge, the corresponding TE sponge will generate a voltage signal due to the occurrence of ΔT

https://doi.org/10.1021/acs.nanolett.2c00696
Nano Lett. 2022, 22, 3417−3424

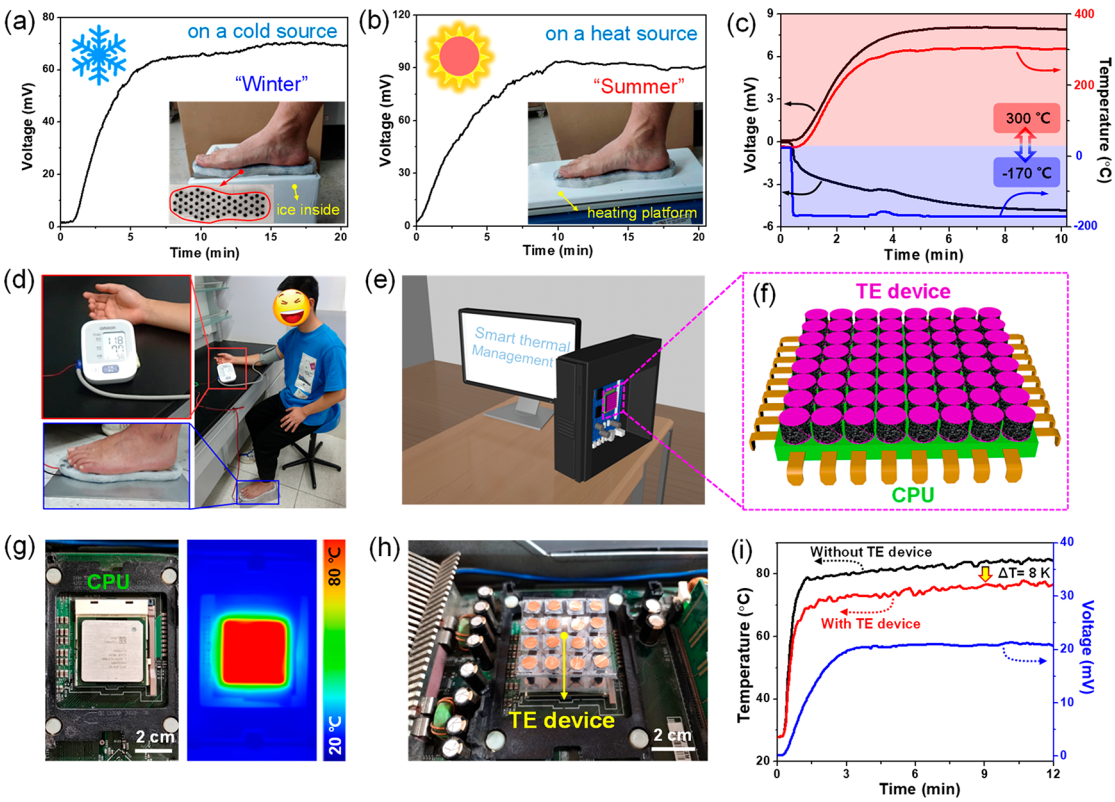

Figure 5. Application of the TE sponge array device. (a, b) The output voltage of the integrated TE device is placed on a cold source of 0 °C (a) and a heat source of 70 °C (b) to simulate the cold and hot environments; the insets show the corresponding optical images of the testing devices. (c) Output voltage of the sponge under extremely high/low-temperature conditions. (d) Application of the integrated TE device for driving a sphygmomanometer by harvesting human thermal energy. (e, f) Schematic diagram of computer equipment (e) with the CPU surface covered with an array TE device (f) for power generation and cooling the CPU. (g) Optical image of a CPU and corresponding infrared image at work with the surface temperature of 85 °C. (h) Optical image of a 4 × 4 array TE device placed on the surface of a normal working CPU. (i) Time-dependent temperature curves and corresponding TE voltage curve, indicating the temperature reduction of ∼8 K when the CPU was covered with the 4 × 4 array TE device.

between the upper and the lower electrodes. While the fingertip leaves the sponge, the TE signal will gradually decrease (Figure 3f). The recovery time of 35 s is larger than the response time due to the long thermal equilibrium time in the recovery process. We designed a multichannel 4 × 4 array TE sensing system based on 16 cylindrical TE sponges as temperature sensors (diameter: 10 mm, height: 3 mm, copper plate as electrodes) embedded in PDMS as a flexible matrix (Figure S10). The TE sponge shows excellent output stability and temperature sensing performance through the finger touching tests. Moreover, a hot iron disk as the heat source and a cold iron disk as the cold source were put on the surfaces of Sensor-1 and Sensor-4. Figure 3g,h exhibit the corresponding 2D and 3D infrared images, respectively. It is observed that the temperatures of the heat and cold sources are approximately 60 °C and −30 °C, which generated the TE voltage of 0.9 mV and −1.5 mV, respectively (Figure 3i). Since there is no obvious ΔT of other channels, it is no significant voltage output, corresponding to the voltage mapping image of the same color. Based on the above research concept, the TE array device with sufficient channels provides a huge potential application concept in signal sensing, position determination, even information security, etc.

Figure 4 shows the excellent TE performance and the huge application potential in the daily life of TE sponges through harvesting human thermal energy. As a stable heat source, the human body can provide continuous thermal energy. And by efficiently collecting heat energy from the human body, it has huge application potential in the development of wearable electronics. The fabricated TE sponge shows good compressive strength and superelasticity, so it is desirable to integrate TE sponge array insoles to harvest and convert human thermal energy into electricity for driving low-power medical equipment (sphygmomanometer, heart rate belt, finger clip oximeter, etc.).

To demonstrate the potential application of the TE sponge, we fabricated an insole-shaped TE sponge array by integrating 62 sponges serially connected into a pearl cotton foam (Figure S11a). The entire insole-shaped TE device can act as both the insole and the sole of a shoe (Figure S11b), and it is hoped that such a smart TE shoe could be designed to generate electricity from the temperature difference between the human body and the external environment. To simulate the cold and hot environments, the integrated TE device was placed on the surface of an ice-box (∼0 °C) and a heating platform (∼70 °C), respectively; as shown in Figure 5a,b, the integrated TE device can deliver stable TE voltage output of ∼70 and 90 mV. Note in some extremely cold regions, the ΔT between indoor and outdoor is even larger, which can better reflect the potential value of the TE sponge, such as in the city of Genhe, Inner Mongolia Autonomous Region of China, where the annual average temperature is about −5 °C and the lowest temperature outdoors is below −50 °C.[59] Therefore, a relatively high ΔT between the human body and the outside

https://doi.org/10.1021/acs.nanolett.2c00696
Nano Lett. 2022, 22, 3417−3424

environment can be obtained, as a satisfactory heat source, showing huge application potential in thermoelectric conversion. To explore the working temperature span of the graphene-based TE sponge, a heating platform and liquid nitrogen were used for designing a stable heat source and cold source. The test was conducted by placing a single TE sponge on top of the heat or cold source, respectively; as shown in Figure 5c, the sponge can still deliver a high and stable output voltage even in such a large temperature span from −170 to 300 °C without obvious structure damage, indicating the excellent stability. To demonstrate the practicability of the integrated TE device in an insole (Figure S11a), the case with a volunteer stepping on a hot metal plate with a temperature of 50 °C has been studied. Through a voltage amplifier system,[23,60,61] the produced electricity can successfully drive low-power medical equipment for monitoring physiological signals (Figure 5d and Figure S11c,d, Note S5). Herein, we expect that if the optimized TE sponges could be integrated into houses in perennial low-temperature areas, there should be wide application potential to take advantage of the large ΔT between indoor and outdoor.

As the total power consumption of electronic devices continues to increase, the rate of device failure caused by overheating is becoming the main failure mode.[62] In addition, when the working temperature exceeds 70 °C, the performance of the electronic device decreases by about 10% for every 2 °C increase in the working temperature.[63] As the most important core component in a computer, the Central Processing Unit (CPU) generates enormous amounts of heat energy, which seriously affects the operating speed and working stability of the computer. As mentioned above, TE materials can achieve the conversion between heat and electricity, so it may be feasible to use TE devices to generate electricity. Meanwhile, the TE sponge can be used as also the heat sink to cool the CPU. As depicted in Figure 5e,f, an array TE device is expected to cover the surface of the CPU and produce TE electricity and then take away heat and radiate it into the air to cool the CPU. Figure 5g shows the optical image and corresponding infrared image of the CPU during operation. The surface temperature of the CPU is as high as 85 °C, and the temperature variation of the CPU surface at different stages in the computer startup process is displayed in Figure S12. To verify the performance of power generation and CPU cooling through a TE device, a 4 × 4 array TE device was fabricated and fixed on the surface of the CPU, and the corresponding photograph is exhibited in Figure 5h. Figure 5i shows the time-dependent temperature and TE voltage curves, and the TE device can provide a relatively stable TE voltage of ∼21 mV. Compared with the condition without the TE device, the temperature of the CPU covered by the 4 × 4 array TE device drops by about 8 K from 84.6 to 76.6 °C. This confirms the practical application potential of the TE array device in daily life, providing a feasible strategy for the TE sponge array to generate electricity and cool electronic devices at the same time.

In summary, we designed a multifunctional superelastic graphene-based TE sponge with a large Seebeck coefficient and compressive strain as high as 49.2 μV/K and 98%, respectively. After 10 000 times cyclic compression at 30% strain, the sponge retains excellent mechanical and thermoelectric stability, and the retention rate of the Seebeck coefficient is still as high as 92.5%. The electrical energy generated by the Seebeck effect can realize self-powered temperature and strain sensing, which corresponds to a high resolution of 0.1 K and a large strain sensitivity of 645.5 nA/% under the ΔT of 16 K. In addition, the sponge can still maintain superior TE stability even in such a large temperature span between −170 and 300 °C. As a wearable device, the sponge array integrated into the insole showed good TE performance in the simulated winter and summer environment and can drive medical equipment for monitoring physiological signals. A 4 × 4 array TE device placed on the surface of a normal working CPU can generate a stable voltage and simultaneously reduce the CPU temperature by 8 K, which provides a feasible strategy for simultaneous power generation and thermal management.

■ ASSOCIATED CONTENT

Supporting Information

The Supporting Information is available free of charge at https://pubs.acs.org/doi/10.1021/acs.nanolett.2c00696.

Details of materials, experimental methods, and SEM characterization; SEM images, mechanical and electrical performance measurement; and application test of the wearable TE device (PDF)

■ AUTHOR INFORMATION

Corresponding Authors

Rujun Ma − *School of Materials Science and Engineering, and National Institute for Advanced Materials, Nankai University, Tianjin 300350, P. R. China*; orcid.org/0000-0001-7892-5212; Email: malab@nankai.edu.cn

Yongsheng Chen − *Center for Nanoscale Science and Technology and Key Laboratory of Functional Polymer Materials, State Key Laboratory and Institute of Elemento-Organic Chemistry, College of Chemistry, Nankai University, Tianjin 300071, P. R. China*; orcid.org/0000-0003-1448-8177; Email: yschen99@nankai.edu.cn

Authors

Ding Zhang − *School of Materials Science and Engineering, and National Institute for Advanced Materials, Nankai University, Tianjin 300350, P. R. China*

Yin Mao − *School of Materials Science and Engineering, and National Institute for Advanced Materials, Nankai University, Tianjin 300350, P. R. China*

Peijia Bai − *School of Materials Science and Engineering, and National Institute for Advanced Materials, Nankai University, Tianjin 300350, P. R. China*

Qi Li − *School of Materials Science and Engineering, and National Institute for Advanced Materials, Nankai University, Tianjin 300350, P. R. China*

Wen He − *School of Materials Science and Engineering, and National Institute for Advanced Materials, Nankai University, Tianjin 300350, P. R. China*

Heng Cui − *School of Materials Science and Engineering, and National Institute for Advanced Materials, Nankai University, Tianjin 300350, P. R. China*

Fei Ye − *School of Materials Science and Engineering, and National Institute for Advanced Materials, Nankai University, Tianjin 300350, P. R. China*

Chenxi Li − *Center for Nanoscale Science and Technology and Key Laboratory of Functional Polymer Materials, State Key Laboratory and Institute of Elemento-Organic Chemistry, College of Chemistry, Nankai University, Tianjin 300071, P. R. China*

Complete contact information is available at:

https://pubs.acs.org/10.1021/acs.nanolett.2c00696

Notes

The authors declare no competing financial interest.

■ ACKNOWLEDGMENTS

This work is supported by the National Key R&D Program of China (Grant Nos. 2020YFA0711500 and 2020YFA0711501), the National Natural Science Fund of China (51973095, 52011540401), and the fellowship of China Postdoctoral Science Foundation (2021T140340).

■ ABBREVIATIONS

TE, thermoelectric; CPU, central processing unit; CNTs, carbon nanotubes; 3D, three-dimensional; 2D, two-dimensional; NaCl, sodium chloride; PDMS, polydimethylsiloxane; Al, aluminum; SEM, scanning electron microscopy; ΔT, temperature difference; TEM, transmission electron microscopy; PF, power factor; RGO, reduced graphene oxide; PVA, poly(vinyl alcohol); PVDF, polyvinylidene fluoride; PU, polyurethane; SpO_2, oxyhemoglobin saturation

■ REFERENCES

(1) Lu, Y.; Qiu, Y.; Cai, K.; Ding, Y.; Wang, M.; Jiang, C.; Yao, Q.; Huang, C.; Chen, L.; He, J. Ultrahigh Power Factor and Flexible Silver Selenide-based Composite Film for Thermoelectric Devices. *Energy Environ. Sci.* **2020**, *13*, 1240.

(2) Ding, T.; Chan, K.; Zhou, Y.; Wang, X.; Cheng, Y.; Li, T.; Ho, G. Scalable Thermoelectric Fibers for Multifunctional Textile-Electronics. *Nat. Commun.* **2020**, *11*, 6006.

(3) Wang, Y.; Yang, L.; Shi, X.-L.; Shi, X.; Chen, L.; Dargusch, M.; Zou, J.; Chen, Z.-G. Flexible Thermoelectric Materials and Generators: Challenges and Innovations. *Adv. Mater.* **2019**, *31*, 1807916.

(4) Peng, J.; Witting, I.; Geisendorfer, N.; Wang, M.; Chang, M.; Jakus, A.; Kenel, C.; Yan, X.; Shah, R.; Snyder, G.; et al. 3D Extruded Composite Thermoelectric Threads for Flexible Energy Harvesting. *Nat. Commun.* **2019**, *10*, 5590.

(5) Ding, Y.; Qiu, Y.; Cai, K.; Yao, Q.; Chen, S.; Chen, L.; He, J. High Performance N-type Ag_2Se Film on Nylon Membrane for Flexible Thermoelectric Power Generator. *Nat. Commun.* **2019**, *10*, 841.

(6) Zhang, D.; Wang, Y.; Yang, Y. Design, Performance, and Application of Thermoelectric Nanogenerators. *Small* **2019**, *15*, 1805241.

(7) Tarascon, J.; Armand, M. Issues and Challenges Facing Rechargeable Lithium Batteries. *Nature* **2001**, *414*, 359.

(8) He, W.; Fu, X.; Bai, P.; Zhang, D.; Cui, H.; Ma, R. High-Performance Coaxial Asymmetry Fibrous Supercapacitors with a Poly (vinyl alcohol)-Montmorillonite Separator. *Nano Lett.* **2021**, *21*, 9164.

(9) Zhu, Y.; Murali, S.; Stoller, M.; Ganesh, K.; Cai, W.; Ferreira, P.; Pirkle, A.; Wallace, R.; Cychosz, K.; Thommes, M.; et al. Carbon-based Supercapacitors Produced by Activation of Graphene. *Science* **2011**, *332*, 1537.

(10) Zhu, H.; Xiao, C.; Xie, Y. Design of Highly Efficient Thermoelectric Materials: Tailoring Reciprocal-Space Properties by Real-Space Modification. *Adv. Mater.* **2018**, *30*, 1802000.

(11) Yang, L.; Chen, Z.-G.; Dargusch, M.; Zou, J. High Performance Thermoelectric Materials: Progress and Their Applications. *Adv. Energy Mater.* **2018**, *8*, 1701797.

(12) Kishore, R.; Nozariasbmarz, A.; Poudel, B.; Sanghadasa, M.; Priya, S. Ultra-high Performance Wearable Thermoelectric Coolers with Less Materials. *Nat. Commun.* **2019**, *10*, 1765.

(13) Zhou, Y.; Zhao, L.-D. Promising Thermoelectric Bulk Materials with 2D Structures. *Adv. Mater.* **2017**, *29*, 1702676.

(14) Zhou, W.; Fan, Q.; Zhang, Q.; Cai, L.; Li, K.; Gu, X.; Yang, F.; Zhang, N.; Wang, Y.; Liu, H.; et al. High-Performance and Compact-Designed Flexible Thermoelectric Modules Enabled by a Reticulate Carbon Nanotube Architecture. *Nat. Commun.* **2017**, *8*, 14886.

(15) Lu, Y.; Qiu, Y.; Jiang, Q.; Cai, K.; Du, Y.; Song, H.; Gao, M.; Huang, C.; He, J.; Hu, D. Preparation and Characterization of Te/Poly(3,4-ethylenedioxythiophene):Poly(styrenesulfonate)/Cu_7Te_4 Ternary Composite Films for Flexible Thermoelectric Power Generator. *ACS Appl. Mater. Interfaces* **2018**, *10*, 42310.

(16) Song, F.; Wu, L.; Liang, S. Giant Seebeck Coefficient Thermoelectric Device of MnO_2 Powder. *Nanotechnology* **2012**, *23*, 085401.

(17) Choi, J.; Jung, Y.; Yang, S.; Oh, J.; Oh, J.; Jo, K.; Son, J.; Moon, S.; Park, C.; Kim, H. Flexible and Robust Thermoelectric Generators Based on All-Carbon Nanotube Yarn without Metal Electrodes. *ACS Nano* **2017**, *11*, 7608.

(18) Kim, C.; Yang, H.; Lee, J.; Lee, G.; Choi, H.; Kim, Y.; Lim, S.; Cho, S.; Cho, B. Self-Powered Wearable Electrocardiography Using a Wearable Thermoelectric Power Generator. *ACS Energy Lett.* **2018**, *3*, 501.

(19) Lee, B.; Cho, H.; Park, K.; Kim, J.-S.; Park, M.; Kim, H.; Hong, Y.; Chung, S. High-Performance Compliant Thermoelectric Generators with Magnetically Self-Assembled Soft Heat Conductors for Self-Powered Wearable Electronics. *Nat. Commun.* **2020**, *11*, 5948.

(20) Jung, K.; Jung, Y.; Choi, C.; Lee, J.; Ko, J. Flexible Thermoelectric Generator with Polydimethyl Siloxane in Thermoelectric Material and Substrate. *Curr. Appl. Phys.* **2016**, *16*, 1442.

(21) Kim, S.; Lee, H.; Choi, H.; Kim, Y.; We, J.; Shin, J.; Lee, K.; Cho, B. High-Performance Flexible Thermoelectric Power Generator Using Laser Multiscanning Lift-Off Process. *ACS Nano* **2016**, *10*, 10851.

(22) Ding, Y.; Xu, W.; Wang, W.; Fong, H.; Zhu, Z. Scalable and Facile Preparation of Highly Stretchable Electrospun PEDOT:PSS@PU Fibrous Nonwovens toward Wearable Conductive Textile Applications. *ACS Appl. Mater. Interfaces* **2017**, *9*, 30014.

(23) Li, M.; Chen, J.; Zhong, W.; Luo, M.; Wang, W.; Qing, X.; Lu, Y.; Liu, Q.; Liu, K.; Wang, Y.; et al. Large-Area, Wearable, Self-Powered Pressure-Temperature Sensor Based on 3D Thermoelectric Spacer Fabric. *ACS Sensors* **2020**, *5*, 2545.

(24) Du, Y.; Cai, K.; Chen, S.; Wang, H.; Shen, S.; Donelson, R.; Lin, T. Thermoelectric Fabrics: toward Power Generating Clothing. *Sci. Rep.* **2015**, *5*, 6411.

(25) Juntunen, T.; Jussila, H.; Ruoho, M.; Liu, S.; Hu, G.; Albrow-Owen, T.; Ng, L.; Howe, R.; Hasan, T.; Sun, Z.; Tittonen, I. Inkjet Printed Large-Area Flexible Few-Layer Graphene Thermoelectrics. *Adv. Funct. Mater.* **2018**, *28*, 1800480.

(26) Feng, S.; Yao, T.; Lu, Y.; Hao, Z.; Lin, S. Quasi-Industrially Produced Large-Area Microscale Graphene Flakes Assembled Film with Extremely High Thermoelectric Power Factor. *Nano Energy* **2019**, *58*, 63.

(27) Nunna, R.; Qiu, P.; Yin, M.; Chen, H.; Hanus, R.; Song, Q.; Zhang, T.; Chou, M.-Y.; Agne, M.; He, J.; et al. Ultrahigh Thermoelectric Performance in Cu_2Se-based Hybrid Materials with Highly Dispersed Molecular CNTs. *Energy Environ. Sci.* **2017**, *10*, 1928.

(28) Kim, J.; Lee, W.; Kang, Y.; Cho, S. Y.; Jang, K. Wet-Spinning and Post-Treatment of CNT/PEDOT:PSS Composites for Use in Organic Fiber-based Thermoelectric Generators. *Carbon* **2018**, *133*, 293.

(29) Yu, C.; Choi, K.; Yin, L.; Grunlan, J. Light-Weight Flexible Carbon Nanotube Based Organic Composites with Large Thermoelectric Power Factors. *ACS Nano* **2011**, *5*, 7885.

(30) Zhang, D.; Song, Y.; Ping, L.; Xu, S.; Yang, D.; Wang, Y.; Yang, Y. Photo-Thermoelectric Effect Induced Electricity in Stretchable Graphene-Polymer Nanocomposites for Ultrasensitive Strain Sensing. *Nano Res.* **2019**, *12*, 2982.

(31) Zhao, X.; Zhang, D.; Xu, S.; Qian, W.; Han, W.; Yang, Y. Self-Powered Wireless Monitoring of Obstacle Position and State in Gas

Pipe via Flow-Driven Triboelectric Nanogenerators. *Adv. Mater. Technol.* **2020**, *5*, 2000466.
(32) Zhao, X.; Zhang, D.; Xu, S.; Qian, W.; Han, W.; Wang, Z.; Yang, Y. Stretching-Enhanced Triboelectric Nanogenerator for Efficient Wind Energy Scavenging and Ultrasensitive Strain Sensing. *Nano Energy* **2020**, *75*, 104920.
(33) Zhao, W.; Fan, S.; Xiao, N.; Liu, D.; Tay, Y.; Yu, C.; Sim, D.; Hng, H.; Zhang, Q.; Boey, F.; Ma, J.; Zhao, X.; Zhang, H.; Yan, Q. Flexible Carbon Nanotube Papers with Improved Thermoelectric Properties. *Energy Environ. Sci.* **2012**, *5*, 5364.
(34) Yao, C.; Zhang, H.; Zhang, Q. Recent Progress in Thermoelectric Materials Based on Conjugated Polymers. *Polymers* **2019**, *11*, 107.
(35) Zhang, Y.; Zhang, Q.; Chen, G. Carbon and Carbon Composites for Thermoelectric Applications. *Carbon Energy* **2020**, *2*, 408.
(36) Zhang, C.; Zhang, Q.; Zhang, D.; Wang, M.; Bo, Y.; Fan, X.; Li, F.; Liang, J.; Huang, Y.; Ma, R.; Chen, Y. Highly Stretchable Carbon Nanotubes/Polymer Thermoelectric Fibers. *Nano Lett.* **2021**, *21*, 1047.
(37) Zhang, D.; Zhang, K.; Wang, Y.; Wang, Y.; Yang, Y. Thermoelectric Effect Induced Electricity in Stretchable Graphene-Polymer Nanocomposites for Ultrasensitive Self-Powered Strain Sensor System. *Nano Energy* **2019**, *56*, 25.
(38) Kim, F.; Yang, S.; Ju, H.; Choo, S.; Lee, J.; Kim, G.; Jung, S.; Kim, S.; Cha, C.; Kim, K.; et al. Direct Ink Writing of Three-Dimensional Thermoelectric Microarchitectures. *Nat. Electron.* **2021**, *4*, 579.
(39) Zeng, W.; Tao, X.-M.; Lin, S.; Lee, C.; Shi, D.; Lam, K.-H.; Huang, B.; Wang, Q.; Zhao, Y. Defect-Engineered Reduced Graphene Oxide Sheets with High Electric Conductivity and Controlled Thermal Conductivity for Soft and Flexible Wearable Thermoelectric Generators. *Nano Energy* **2018**, *54*, 163.
(40) Wang, Y.; Yang, J.; Wang, L.; Du, K.; Yin, Q.; Yin, Q. J. Polypyrrole/Graphene/Polyaniline Ternary Nanocomposite with High Thermoelectric Power Factor. *ACS Appl. Mater. Interfaces* **2017**, *9*, 20124.
(41) Wang, L.; Yao, Q.; Bi, H.; Huang, F.; Wang, Q.; Chen, L. Large Thermoelectric Power Factor in Polyaniline/Graphene Nanocomposite Films Prepared by Solution-Assistant Dispersing Method. *J. Mater. Chem. A* **2014**, *2*, 11107.
(42) Park, C.; Yoo, D.; Im, S.; Kim, S.; Cho, W.; Ryu, J.; Kim, J. Large-Scalable RTCVD Graphene/PEDOT:PSS Hybrid Conductive Film for Application in Transparent and Flexible Thermoelectric Nanogenerators. *RSC Adv.* **2017**, *7*, 25237.
(43) Yoo, D.; Kim, J.; Kim, J. H. Direct Synthesis of Highly Conductive Poly(3,4-ethylenedioxythiophene):Poly(4-styrenesulfonate) (PEDOT:PSS)/Graphene Composites and Their Applications in Energy Harvesting Systems. *Nano Res.* **2014**, *7*, 717.
(44) Du, Y.; Cai, K. F.; Shen, S.; Casey, P. Preparation and Characterization of Graphene Nanosheets/Poly(3-hexylthiophene) Thermoelectric Composite Materials. *Synth. Met.* **2012**, *162*, 2102.
(45) Wu, Y.; Yi, N.; Huang, L.; Zhang, T.; Fang, S.; Chang, H.; Li, N.; Oh, J.; Lee, J.; Kozlov, M.; Chipara, A.; Terrones, H.; Xiao, P.; Long, G.; Huang, Y.; Zhang, F.; Zhang, L.; Lepró, X.; Haines, C.; Lima, M.; Lopez, N.; Rajukumar, L.; Elias, A.; Feng, S.; Kim, S.; Narayanan, N.; Ajayan, P.; Terrones, M.; Aliev, A.; Chu, P.; Zhang, Z.; Baughman, R.; Chen, Y. Three-Dimensionally Bonded Spongy Graphene Material with Super Compressive Elasticity and Near-Zero Poisson's Ratio. *Nat. Commun.* **2015**, *6*, 6141.
(46) Ren, H.; Tang, M.; Guan, B.; Wang, K.; Yang, J.; Wang, F.; Wang, M.; Shan, J.; Chen, Z.; Wei, D.; Liu, Z.; et al. Hierarchical Graphene Foam for Efficient Omnidirectional Solar-Thermal Energy Conversion. *Adv. Mater.* **2017**, *29*, 1702590.
(47) Yang, H.; Li, Z.; Lu, B.; Gao, J.; Jin, X.; Sun, G.; Zhang, G.; Zhang, P.; Qu, L. Reconstruction of Inherent Graphene Oxide Liquid Crystals for Large-Scale Fabrication of Structure-Intact Graphene Aerogel Bulk toward Practical Applications. *ACS Nano* **2018**, *12*, 11407.
(48) Si, Y.; Wang, X.; Dou, L.; Yu, J.; Ding, B. Ultralight and Fire-Resistant Ceramic Nanofibrous Aerogels with Temperature-Invariant Superelasticity. *Sci. Adv.* **2018**, *4*, eaas8925.
(49) Xie, Y.; Xu, S.; Xu, Z.; Wu, H.; Deng, C.; Wang, X. Interface-Mediated Extremely Low Thermal Conductivity of Graphene Aerogel. *Carbon* **2016**, *98*, 381.
(50) Xu, S.; Qian, W.; Zhang, D.; Zhao, X.; Zhang, X.; Li, C.; Bowen, C.; Yang, Y. A Coupled Photo-Piezo-Catalytic Effect in a BST-PDMS Porous Foam for Enhanced Dye Wastewater Degradation. *Nano Energy* **2020**, *77*, 105305.
(51) Qian, W.; Zhao, K.; Zhang, D.; Bowen, C.; Wang, Y.; Yang, Y. Piezoelectric Material-Polymer Composite Porous Foam for Efficient Dye Degradation via the Piezo-Catalytic Effect. *ACS Appl. Mater. Interfaces* **2019**, *11*, 27862.
(52) Liu, Y.; Liu, Z.; Lew, W.; Wang, Q. Temperature Dependence of the Electrical Transport Properties in Few-Layer Graphene Interconnects. *Nanoscale Res. Lett.* **2013**, *8*, 335.
(53) Kim, H.; Na, G.; Kwon, Y.; Kang, S.; Choi, M.; Bang, J.; Wu, P.; Kim, S. Microwave-Assisted Synthesis of Graphene-SnO_2 Nanocomposites and Their Applications in Gas Sensors. *ACS Appl. Mater. Interfaces* **2017**, *9*, 31667.
(54) Zhang, D.; Xu, S.; Zhao, X.; Qian, W.; Bowen, C.; Yang, Y. Wireless Monitoring of Small Strains in Intelligent Robots via a Joule Heating Effect in Stretchable Graphene-Polymer Nanocomposites. *Adv. Funct. Mater.* **2020**, *30*, 1910809.
(55) Du, T.; Xiong, Z.; Delgado, L.; Liao, W.; Peoples, J.; Kantharaj, R.; Chowdhury, P.; Marconnet, A.; Ruan, X. Wide Range Continuously Tunable and Fast Thermal Switching Based on Compressible Graphene Composite Foams. *Nat. Commun.* **2021**, *12*, 4915.
(56) Guo, Y.; Mu, J.; Hou, C.; Wang, H.; Zhang, Q.; Li, Y. Flexible and Thermostable Thermoelectric Devices Based on Large-Area and Porous All-Graphene Films. *Carbon* **2016**, *107*, 146.
(57) Gao, J.; Liu, C.; Miao, L.; Wang, X.; Peng, Y.; Chen, Y. Enhanced Power Factor in Flexible Reduced Graphene Oxide/Nanowires Hybrid Films for Thermoelectrics. *RSC Adv.* **2016**, *6*, 31580.
(58) Du, Y.; Shen, S.; Yang, W.; Donelson, R.; Cai, K.; Casey, P. Simultaneous Increase in Conductivity and Seebeck Coefficient in a Polyaniline/graphene Nanosheets Thermoelectric Nanocomposite. *Synth. Met.* **2012**, *161*, 2688.
(59) Ren, J.; Shen, Z.; Yang, J.; Zhao, J.; Yin, J. Effects of Temperature and Dry Density on Hydraulic Conductivity of Silty Clay under Infiltration of Low-Temperature Water. *Arabian J. Sci. Eng.* **2014**, *39*, 461.
(60) Lei, Z.; Gao, W.; Wu, P. Double-Network Thermocells with Extraordinary Toughness and Boosted Power Density for Continuous Heat Harvesting. *Joule* **2021**, *5*, 2211.
(61) Gao, W.; Lei, Z.; Zhang, C.; Liu, X.; Chen, Y. Stretchable and Freeze-Tolerant Organohydrogel Thermocells with Enhanced Thermoelectric Performance Continually Working at Subzero Temperatures. *Adv. Funct. Mater.* **2021**, *31*, 2104071.
(62) Gan, T.; Ming, T.; Fang, W.; Liu, Y.; Miao, L.; Ren, K.; Ahmadi, M. Heat Transfer Enhancement of a Microchannel Heat Sink with The Combination of Impinging Jets, Dimples, and Side Outlets. *J. Therm. Anal. Calorim.* **2020**, *141*, 45.
(63) Cui, H.; Zhang, Q.; Bo, Y.; Bai, P.; Wang, M.; Zhang, C.; Qian, X.; Ma, R. Flexible Microfluidic Electrocaloric Cooling Capillary Tube with Giant Specific Device Cooling Power Density. *Joule* **2022**, *6*, 258.

https://doi.org/10.1021/acs.nanolett.2c00696
Nano Lett. 2022, 22, 3417−3424